

SIXTH EUROPEAN ROTORCRAFT AND POWERED LIFT AIRCRAFT FORUM

Paper No. 47

THEORETICAL PREDICTION OF DYNAMIC-INFLOW DERIVATIVES

Dale M. Pitt

U.S. Army Aviation Research and Development Command
St. Louis, MO 63166 USA

David A. Peters

Washington University, Box 1185
St. Louis, MO 63130 USA

September 16-19, 1980
Bristol, England

THE UNIVERSITY, BRISTOL, BS8 1HR, ENGLAND

THEORETICAL PREDICTION OF
DYNAMIC-INFLOW DERIVATIVES

Dale M. Pitt
U.S. Army AVRADCOM
St. Louis, Missouri, USA

David A. Peters
Washington University
St. Louis, Missouri, USA

ABSTRACT

A linear, unsteady theory is developed that relates transient rotor loads (thrust, roll moment, and pitch moment) to the overall transient response of the rotor induced-flow field. The relationships are derived from an unsteady, actuator-disc theory; and some are obtained in closed form. The results reveal both the strengths and weaknesses of previous formulations, and the results also indicate areas in which further study is needed.

1. Introduction

It has been known for some thirty years that the induced-flow field associated with a lifting rotor responds in a dynamic fashion to changes in either blade pitch (i.e. pilot inputs) or rotor flapping angles (i.e. rotor or body dynamics,) Refs. 1-3. In recent years, it has been found that dynamic inflow for steady response in hover can be treated by an equivalent (i.e. reduced) Lock number, Ref. 4. For more general conditions, such as transient motions or a rotor in forward flight, it has been determined that the induced flow can be treated by additional "degrees of freedom" of the system. Each degree of freedom represents a particular inflow distribution, and each has its own particular gain and time constant, Refs. 5-7.

Although the above results have provided some impressive correlation with experimental data, there is still no general theory to predict the gains and time-constants of dynamic inflow. Values from momentum theory give excellent results in hover, but are clearly inadequate in forward flight, Refs. 5-6. A simple vortex model, Ref. 5, gives some improvement in forward flight but is still not satisfactory. An empirical model based on the best fit of response data, Refs. 5-6, gives excellent results; but several peculiar singularities remain unexplained. Thus, there is a need to determine the dynamic-inflow behavior from fundamental, aerodynamic considerations. One type of analysis that appears capable of producing such results is actuator-disc theory, Refs. 8-10. Although this type of analysis has been used extensively for induced-flow calculation, it has not been used to obtain the necessary gains and time constants required for dynamic inflow. There are primarily two reasons for this neglected application. First, most investigators have been interested in the details of the wake for a steady flight condition (rather than in the dynamic properties of the wake due to perturbations in flight condition). Second, investigators often include the coupled response of blade motions in their analysis. This hopelessly complicates the analysis and precludes the type of results desired here.

Figure 1 gives a schematic representation of the coupled inflow/rotor problem. The inflow dynamics and rotor dynamics of the closed-loop system are strongly coupled. It is the purpose of this paper, however, to investigate the behavior (i.e. the transfer function) of the open-loop induced flow

model. The resultant theory may then be used with any model of the rotor dynamics. To do this, we extend the actuator-disc theory of Ref. 9 to the unsteady case and use it to find the dynamic relationships between the aerodynamic loading and the induced flow. Special emphasis is placed in developing these relationships in terms of a first-order dynamic model for each inflow distribution.

2. Background

The theory of dynamic inflow relates the airloads of a rotor (C_T , C_L , and C_M) to the induced-flow distributions (λ_o , λ_s , λ_c) where C_T , C_L , and C_M are the aerodynamic perturbation in thrust, roll moment, and pitch moment; and λ_o , λ_s , and λ_c are the magnitudes of uniform, side-to-side, and fore-to-aft variations in induced flow.

$$\lambda = \lambda_o + \lambda_s r \sin\psi + \lambda_c r \cos\psi \quad (1)$$

(Note that even rotors with no net hub moment can have considerable aerodynamic moments which, although balanced by inertial moments in the rotor system, can nevertheless influence the induced flow.) The dynamic inflow models of Refs. 6-7 assume that the inflow is related to the aerodynamic loads in a linear, first-order fashion.

$$\begin{bmatrix} M \end{bmatrix} \begin{bmatrix} \lambda_o \\ \lambda_s \\ \lambda_c \end{bmatrix} + \begin{bmatrix} L \end{bmatrix}^{-1} \begin{bmatrix} \lambda_o \\ \lambda_s \\ \lambda_c \end{bmatrix} = \begin{bmatrix} C_T \\ C_L \\ C_M \end{bmatrix} \quad (2a)$$

or

$$\begin{bmatrix} \tau \end{bmatrix} \begin{bmatrix} \lambda_o \\ \lambda_s \\ \lambda_c \end{bmatrix} + \begin{bmatrix} \lambda_o \\ \lambda_s \\ \lambda_c \end{bmatrix} = \begin{bmatrix} L \end{bmatrix} \begin{bmatrix} C_T \\ C_L \\ C_M \end{bmatrix} \quad (2b)$$

The purpose of this research is to find the elements of [L] and [M] from basic aerodynamic principles and to also investigate the validity of this linear, first-order form.

The actuator-disc theory that we use in this investigation is based on pressure distributions developed by Kinner (see Ref. 9). Kinner discovered a family of pressure distributions that solve Laplace's equation, $\phi_{,ii} = 0$, and that also give a pressure discontinuity (i.e. lift) across a circular disc. These distributions can be combined in a general form to give the total, nondimensional pressure ϕ

$$\phi = \sum_{\substack{m,n=0 \\ m < n}}^{\infty} P_n^m(\nu) Q_n^m(i\eta) [C_n^m \cos m\psi + D_n^m \sin m\psi] \quad (3)$$

where P_n^m and Q_n^m are, respectively, associated Legendre functions of the first and second kinds; C_n^m and D_n^m are arbitrary constants; and ν , η , and ψ are ellipsoidal coordinates defined by the relationships

$$x = -\sqrt{1-\nu^2} \sqrt{1+\eta^2} \cos\psi \quad (4a)$$

$$y = \sqrt{1-\nu^2} \sqrt{1+\eta^2} \sin\psi \quad (4b)$$

$$z = -\nu\eta \quad (4c)$$

where Z is normal to the rotor plane and positive down; X is in the rotor plane and positive in the forward direction, $\psi = 180^\circ$; and Y is in the rotor plane and positive in the starboard direction, $\psi = 90^\circ$. On the rotor disc, $\eta = 0$, $v = \sqrt{1-r^2}$, and ψ is the conventional, counterclockwise azimuth angle. A schematic of the coordinate system is given in Figure 2.

The nondimensional aerodynamic loading can be calculated from the nondimensional pressure, $\phi = \text{pressure}/\rho\Omega^2R^2$, by use of the following integrals, taken over the rotor disc.

$$C_T = \iint \phi dA = \frac{4}{3} C_1^0 \quad (5a)$$

$$C_L = \iint \phi(-r\sin\psi) dA = \frac{8}{5} i D_2^1 \quad (5b)$$

$$C_M = \iint \phi(-r\cos\psi) dA = \frac{8}{5} i C_2^1 \quad (5c)$$

The variables r and dA are nondimensional ($0 \leq r \leq 1$, $\iint dA = \pi$). For the sake of later comparisons, we also introduce two second-harmonic pressure integrals.

$$C_{L2} \equiv \iint \phi(-r^2\sin 2\psi) da = \frac{128}{7} D_3^2 \quad (5d)$$

$$C_{M2} \equiv \iint \phi(-r^2\cos 2\psi) dA = \frac{128}{7} C_3^2 \quad (5e)$$

It is interesting to note that each loading integral in equation (5) is uniquely determined by a single coefficient of the Kinner distribution and is independent of all others. Therefore, differing pressure distributions can result in identical average loadings. One of the purposes of this research is to find out if such pressure distributions will also result in identical averaged values of the induced flow. To do this, we will consider two types of pressure distribution. The first, called "uncorrected," will contain only the single coefficient of ϕ necessary to create the appropriate loading, as given in equation (5). The second distribution, called "corrected," will include just enough of the next-higher Kinner term to enforce the conditions $\phi = 0$, $d\phi/dr = 0$, at $r = 0$, which is a reasonable distribution for a rotor. The resulting additional terms are C_3^0 , D_4^1 , and C_4^1 . A summary of the pressure terms used in each distribution is given in Table 1, and the corrected and uncorrected distributions are plotted in Figures 3-5 as functions of radial station, r .

The pertinent integrals that define the magnitude of the basic induced-flow distributions at the disc are given by

$$\lambda_o = \frac{1}{\pi} \iint \lambda dA \quad (6a)$$

$$\lambda_s = \frac{4}{\pi} \iint \lambda r \sin\psi dA \quad (6b)$$

$$\lambda_c = \frac{4}{\pi} \iint \lambda r \cos\psi dA \quad (6c)$$

$$\lambda_{2s} = \frac{6}{\pi} \iint \lambda r^2 \sin 2\psi dA \quad (6d)$$

$$\lambda_{2c} = \frac{6}{\pi} \iint \lambda r^2 \cos 2\psi dA \quad (6e)$$

where λ is the nondimensional induced flow (velocity divided by ΩR).

3. Mathematical Formulation

For a free-stream velocity in the negative ξ direction (as shown in Figure 2), the induced velocity components, q_i , must satisfy the continuity and momentum equations,

$$q_{i,i} = 0 \quad (7a)$$

$$q_{i,o} - vq_{i,\xi} = -\phi_{,i} \quad (7b)$$

where ,o implies $d/d(\Omega t)$, and v is the free-stream velocity divided by ΩR . We will now examine several special cases of equation (7) to determine relationships between loading, ϕ , and induced flow normal to the disc, q_z , at $\eta = 0$.

The first case we consider is the steady condition, $q_{i,o} = 0$. Equations (7) become

$$\phi_{,ii} = 0 \quad (8a)$$

$$q_{i,\xi} = \frac{1}{v} \phi_{,i} \quad (8b)$$

Equation (8a), the Laplace equation, implies that the Kinner distribution, equation (3), is an appropriate solution. The normal induced velocity at a point (x_o, y_o) on the rotor disc is found from equation (8b) with $i = z$

$$q_z = \lambda(x_o, y_o) = \frac{1}{v} \int_{\infty}^o \phi_{,z} d\xi \quad (9)$$

where ξ follows the streamline from (x_o, y_o) to infinity,

$$x = x_o + \xi \cos \alpha \quad (10a)$$

$$y = y_o \quad (10b)$$

$$z = -\xi \sin \alpha \quad (10c)$$

and α is the angle of incidence, Figure 2. The z derivative in equation (9) may be expressed in ellipsoidal coordinates.

$$\phi_{,z} = \frac{-\eta(1-v^2)}{v^2+\eta^2} \frac{\partial \phi}{\partial v} - \frac{v(1+\eta^2)}{v^2+\eta^2} \frac{\partial \phi}{\partial \eta} \quad (11)$$

Thus, the induced flow for a given pressure distribution is found by integration of the Kinner functions from the disc to the far field.

A specialization of equation (9) can be made for the condition $\alpha = 90^\circ$ (axial flow). For such a condition z and ξ are parallel; and equation (9) reduces to

$$\lambda = -\frac{1}{v} \phi \Big|_{\eta=0} \quad (12)$$

Thus, the induced flow may be found directly from ϕ with no integration. Another specialization of equation (9) can be made for $\alpha = 0^\circ$ (edgewise flow). Here, ξ is parallel to x ; and a portion of the integration is on the disc.

$$\lambda = -\frac{1}{v} \int_{\infty}^{\sqrt{1-y_0^2}} \frac{1}{\eta} \frac{\partial \phi}{\partial v} \Big|_{v=0} dx - \frac{1}{v} \int_0^{x_0} \frac{1}{v} \frac{\partial \phi}{\partial \eta} \Big|_{\eta=0} \sqrt{1-y_0^2} dx \quad (13)$$

Thus, equation (9) and its two specializations, equations (12) and (13), summarize the steady case, $\omega = 0$.

The second general case we consider is the disc in still air, $v = 0$, with a simple-harmonic pressure distribution, $\phi = \bar{\phi} e^{i\omega\psi}$ where $\psi = \Omega t$ and ω is the oscillatory frequency, nondimensionalized on Ω (i.e. per rev). Equations (7) become, with $q = \bar{q} e^{i\omega\psi}$,

$$\phi_{,ii} = 0 \quad (14a)$$

$$i\omega \bar{q}_i = -\bar{\phi}_{,i} \quad (14b)$$

Equation (14a) indicates that the Kinner distribution is applicable, and equation (14b) gives the induced flow.

$$\bar{q}_z = \frac{i}{\omega} \bar{\phi}_{,z} \quad (15a)$$

$$\lambda = \frac{-i}{\omega} \frac{1}{v} \frac{\partial \bar{\phi}}{\partial \eta} \Big|_{\eta=0} \quad (15b)$$

No integration is required.

The next case we consider is an oscillatory velocity field, $q = \bar{q} e^{i\omega\psi}$, where \bar{q} is taken as real, which implies that all induced velocities are mutually in phase. If we express the pressure as $\phi = (A+Bi)e^{i\omega\psi}$, equation (7) yields

$$A_{,ii} = B_{,ii} = 0 \quad (16a)$$

$$v \bar{q}_{i,\xi} = A_{,i} \quad (\text{real}) \quad (16b)$$

$$\omega \bar{q}_i = -B_{,i} \quad (\text{imaginary}) \quad (16c)$$

Equation (16a) shows that both the real and imaginary portions of ϕ can be represented by Kinner solutions. Equation (16b) shows that real (i.e. in-phase) portion of the pressure relates to induced velocity exactly as does the steady case, equation (8b). Equation (16c) shows that imaginary (i.e. out-of-phase) component of pressure relates to induced velocity exactly as does the case $v = 0$, equation (15a). Therefore, when all induced velocities are mutually in phase, the total pressure is simply a superposition of the steady pressure ($\omega=0$) and the apparent-mass pressure ($v=0$). Thus, the basic assumption of the theory of dynamic inflow, equation (2a), is partially validated.

The final case we consider is an oscillatory pressure field, $\phi = \bar{\phi} e^{i\omega\psi}$, in which all pressures are mutually in phase ($\bar{\phi}$ real). If we express the resultant induced flow as $q = (u+iw)e^{i\omega\psi}$, equations (7) become

$$\bar{\phi}_{,ii} = 0 \quad (17a)$$

$$\omega w_i + v u_{i,\xi} = \bar{\phi}_{,i} \quad (\text{real}) \quad (17b)$$

$$\omega u_i - v w_{i,\xi} = 0 \quad (\text{imaginary}) \quad (17c)$$

Equation (17a) indicates, again, that the Kinner distribution is appropriate. Equations (17b) and (17c) may be combined to give equations for the induced flow in terms of $\bar{\phi}$.

$$\omega^2 u_i + v^2 u_{i,\xi\xi} = v \bar{\phi}_{,i\xi} \quad (18a)$$

$$\omega^2 w_i + v^2 w_{i,\xi\xi} = \omega \bar{\phi}_{,i} \quad (18b)$$

Equations (18) are solved by a Laplace transform in ξ followed by application of the convolution theorem. The final solution for induced flow at the rotor disk is

$$u_z = \frac{1}{v} \int_{-\infty}^{\infty} \bar{\phi}_{,z} \cos(k\xi) d\xi \quad (19a)$$

$$w_z = -\frac{1}{v} \int_{-\infty}^{\infty} \bar{\phi}_{,z} \sin(k\xi) d\xi \quad (19b)$$

where k is a reduced frequency, ω/v , based on air speed (not tip speed).

Equations (19) are very interesting. They show that the in-phase and out-of-phase induced velocities may be calculated in the same manner as the steady case, equation (9), except that weighting functions ($\cos k\xi$ or $-\sin k\xi$) must be added. It should be noted that, since a true rotor should behave somewhere between "in-phase velocities," equations (16); and "in-phase pressures," equations (19), numerical comparisons of these two cases should prove very valuable for the validation of a first-order dynamic-inflow theory.

4. Closed-Form Results

Before proceeding to the numerical results it is good to consider some closed-form solutions. These provide added insights into the characteristics of dynamic inflow, and they also serve as checks on the accuracy of the numerical algorithms. Although we are primarily interested in the 3x3 L and M matrices of equations (2), we will also look at the elements of more general 5x5 matrices obtained by an extension of the induced-flow and loading vectors to include $\langle \lambda_s, \lambda_c, \lambda_{2s}, \lambda_{2c} \rangle$ and $\langle C_T, C_L, C_M, C_{L2}, C_{M2} \rangle$, respectively. The λ 's and C 's are defined by equations (5)_L and (6)_M. The 5x5 matrices include the effect of second-harmonic loads on the induced flow; they give the magnitude of the higher-harmonics of induced flow; and they provide for a five-degree-of-freedom induced-flow model, should the three-degree-of-freedom model prove inadequate for a given system.

We now present closed-form results for several special cases. First, we consider $\omega=0$, $\alpha=90^\circ$ (steady, axial flow). The pertinent theory is given by equation (12). Substitution of equations (3) and (12) into equation (6), with terms defined as in Table 1, yields

$$L_{11} = 1/2v, \quad L_{22} = L_{33} = -2/v, \quad L_{44} = L_{55} = 3/v$$

$$L_{ij} = 0, \quad i \neq j \quad (20a-d)$$

An important property of the results in equation (20) is that elements of L are entirely independent of induced-flow distribution. Thus, they are identical for the corrected and uncorrected pressure distributions. Another interesting aspect of equation (20) is that the L_{11} , L_{22} , and L_{33} elements are identical to those obtained from simple momentum theory, Ref. 6. It would appear that this correspondence is more than coincidental. In particular, the lift-deficiency function obtained from the results in equation (20), (see Ref. 6) is given by

$$\gamma^*/\gamma = \frac{1}{1+\sigma a/8v} \quad (21)$$

and is identical to the lift-deficiency functions obtained by Loewy (from a shed-vorticity analysis) and by Miller (from a vorticity-tube theory), Refs. 10 and 11. Thus, there is an apparent universality in the results for axial flow.

A second special case for which closed-form results can be obtained is $\omega=0$, $\alpha=0^\circ$ (steady, edgewise flow), equation (13). Table 2 lists the closed-form results for both the uncorrected and the corrected pressure distributions, and these are compared with the results of the vortex and momentum theories of Ref. 5. Several conclusions are important here. First, the L_{11} element remains $1/2v$ (as it was for $\alpha=90^\circ$) independent of lift distribution. The L_{22} element is about twice the value predicted by momentum theory, and it is only slightly dependent upon the lift distribution. The L_{33} element is identically zero, independent of lift distribution. The coupling terms, L_{31} (λ_c due to C_T) and L_{13} (λ_o due to C_M), are zero in momentum theory but are present in the vortex and actuator-disc theories. They are definitely affected by the lift distribution, but not qualitatively. Of special interest is the fact that L_{31} is greater than L_{11} , which implies that C_T would create an upwash ($\lambda < 0$) at the leading edge, $\psi=180^\circ$. This is consistent with measurements, Ref. 9. All elements of the 3×3 L-matrix agree qualitatively with the Ormiston vortex model, Ref. 5.

The higher-harmonic elements of L are also interesting. L_{51} (λ_{2c} due to C_T) is highly sensitive to lift distribution and is not at all small. L_{42} (λ_{2s} due to C_s) is much less sensitive to lift distribution but is also substantial. The L_{55} term (λ_{2c} due to C_{M2}) is twice the value of L_{55} for $\alpha=90^\circ$. The only nonzero coupling term is L_{24} (λ_s due to C_{T2}). It is roughly half the value of the diagonal element, L_{22} , (λ_s due to C_T). All elements not listed in Table 2 are identically zero due to conditions of symmetry.

The qualitative differences between the L-matrices for $\alpha=0^\circ$ and $\alpha=90^\circ$ lead to the obvious question as to how the elements vary as functions of α (i.e. how they vary from hover to forward flight). Although we examine this behavior in detail in the next section, there are some closed-form solutions for this variation which are rather useful. In particular, the Fourier components obtained in Ref. 12 can be used to obtain the first column of L. For the corrected lift distribution, these are

$$L_{11} = \frac{1}{2v} \quad (22a)$$

$$L_{31} = \frac{15\pi}{64v} \sqrt{\frac{1-\sin\alpha}{1+\sin\alpha}} \quad (22b)$$

$$L_{51} = -\frac{3}{7v} \left(\frac{1-\sin\alpha}{1+\sin\alpha} \right) \quad (22c)$$

For the uncorrected distributions, the α -variations are the same as in equation (22); but the coefficients are altered, as appropriate, to match $\alpha=0^\circ$. (The L_{11} element is completely independent of lift distribution and angle of incidence.) The variation of L_{31} is approximately linear with α and is identical to the variation obtained from the vortex-element theory of Ref. 13. The variation of L_{51} is smooth, and somewhat parabolic, as α varies from 90° to 0° .

The final closed-form results to be considered are the apparent mass terms for $v=0$, equation (15b). The evaluation of this equation, according to the entries in Table 1, results in the M-matrix given in Table 3. Several points are noteworthy. First, the uncorrected values of M_{11} , M_{22} , and M_{33} are identical to the values obtained for the apparent mass of an impermeable disk, Ref. 6. Second, there are significant differences between results for corrected and uncorrected lift distributions. Therefore the apparent mass terms are more sensitive to pressure distribution than are the steady terms. Third, the apparent mass terms decrease with increasing harmonics of λ .

5. Numerical Results

We now turn to numerical results for the elements of L versus disc angle, α . The ξ integral in equation (9) is calculated by Simpson's 1/3 Rule at intervals varying from .01 to .05 and going out to $\xi=20$. These integrals are used to find $\lambda(r,\psi)$ at 10, unequally-spaced radial stations and at 5° azimuthal increments. The averages in equation (6) are computed by Gauss quadrature in r and by Fourier analysis in ψ . The accuracy of the results may be gauged in the subsequent figures by comparison with the closed-form, starred values of $\alpha=0^\circ$ and $\alpha=90^\circ$.

Figure 6 gives corrected and uncorrected values of the elements of the first column of L (induced flow due to perturbations in C_T). These results can be compared with the closed-form expressions in equation (20); and they show an accuracy of 0.1%, for $5^\circ < \alpha < 90^\circ$, and an accuracy of 4% as α approaches 0° . The results illustrate the smooth transition of all elements even as α approaches 0° , at which point the disc is in its own wake. Figure 7 gives the second column of L (induced flow due to C_r). The L_{22} element is nearly independent of lift distribution for $\alpha > 10^\circ$; but for $\alpha < 10^\circ$ a noticeable difference develops between the corrected and uncorrected values. The L_{42} element displays a dependence on lift distribution that is independent of α . Figure 8 gives the third column of L (induced flow due to C_M). The λ_o component, L_{13} , varies smoothly with α ; and there is a difference between corrected and uncorrected results only for $\alpha < 10^\circ$. The λ_c component, L_{33} , varies smoothly and is nearly independent of pressure distribution. The higher-harmonic component, L_{53} , is zero for both $\alpha = 0^\circ$ and $\alpha = 90^\circ$; but it is nonzero for intermediate angles and reaches a maximum at $\alpha = 30^\circ$.

Figures 9-10 give the effect of second-harmonic loading on the L-matrix. These results can be used to determine if dynamic perturbations in the higher-harmonic loads might cause significant changes in λ_o , λ_s , or λ_c and thereby invalidate the assumptions of dynamic-inflow theory. Figure 9^c shows that

there is some λ due to C_{L2} (i.e. L_{24}), and its maximum value is 2.58 at $\alpha = 0^\circ$. Given, however, that L_{22} is twice this value and that C_{L2} is probably less than half of C_L , it is reasonable to assume that this coupling could be neglected. Figure 9 further shows that both L_{24} and L_{44} vary smoothly with α . Figure 10 shows that L_{15} (λ_0 due to C_{M2}) and L_{35} (λ_c due to C_{M2}) may reasonably be neglected, the former being identically zero for all α , and the latter remaining less than 0.5. L_{55} varies smoothly with α .

The preceding numerical results provide a foundation for the choice of an analytic 3x3 L-matrix. For the first column of this matrix, we use the corrected, closed-form results in equations (22a) and (22b). The corrected lift distribution is used because, from Figure 3, we see that the uncorrected distribution is unrealistic for a lifting rotor. For the second two columns of L, however, we choose the uncorrected results of Figures 7-8. There are several reasons for this choice. First, we seen in Figures 4-5 that either the corrected or the uncorrected distribution for moment is reasonable for the first harmonic variation in lift. Second, Figures 7-8 show that the two distributions give nearly identical results (for L_{13} , L_{33} , and L_{22}) when $\alpha > 10^\circ$. Since helicopters operate with α 's from 5° to 10° , there should be little practical difference between the two distributions. Third, the uncorrected distributions follow smooth curves that appear to be identical to the α -functions in equation (22). Therefore, simple analytic expressions are available for these uncorrected curves. The resultant analytic form of the L-matrix is given in Table 4. The M-matrix, also given in Table 4, is for the identical assumptions. The first column is corrected, and the second two columns are uncorrected. The choice of uncorrected apparent mass for M_{22} and M_{33} is also consistent with experimental results in Ref. 6 that show that these give realistic time constants. There is a certain symmetry to the L-matrix in Table 4 ($L_{13} = L_{31}$ and $L_{11} + L_{22} + L_{33} = \text{constant}$). Furthermore, an eigenvalue analysis of $[L][M]$ shows that there are no anomalies in the system. The induced flow has three real, stable roots for all values of α between 0° and 90° ; and L is always invertible.

6. Extensions and Future Work

There are three major areas in which the preceding results need to be verified or extended. First, the corrected and uncorrected 3x3 and 5x5 models need to be compared in terms of their effect in a coupled, rotor/body dynamic analysis in order to verify the adequacy of the model in Table 4. Second, the results here need to be extended to include the effects of wake contraction and finite number of blades in order to see if these significantly affect the dynamic-inflow model. Third, the complete effect of reduced frequency needs to be investigated with respect to the differences between the assumptions of in-phase velocities and in-phase pressures.

Concerning the effect of wake contraction, there already exists a result from momentum theory that may allow the present results to be directly extended to the lifting case, Ref. 6. In particular, it is suggested that the present value of v ,

$$v = \sqrt{\mu^2 + \bar{\lambda}^2} \quad (\text{no lift}) \quad (23a)$$

be replaced by a more general mass-flow parameter

$$v = \frac{\mu^2 + (\bar{\lambda} + \bar{v})(\bar{\lambda} + 2v)}{\sqrt{\mu^2 + (\bar{\lambda} + \bar{v})^2}} \quad (\text{steady lift}) \quad (23b)$$

where μ is the inplane component of the aircraft velocity (advance ratio), $\bar{\lambda}$ is the normal component of aircraft velocity (inflow ratio), and \bar{v} is the steady induced flow due to rotor thrust. Similarly, the angle α could be defined as the wake skew angle at the rotor.

$$\alpha = \tan^{-1} \frac{\bar{\lambda} + \bar{v}}{\mu} \quad (23c)$$

In order to verify the usefulness of equations (23b) and (23c), as well as the effect of number of blades, we intend to use an existing, prescribed-wake analysis to calculate the steady L-matrix for various contraction ratios and for rotors with a finite number of blades.

Concerning the effect of reduced frequency, we are currently computing the integrals in equation (19) at various values of k . We already know that, for the second and third rows of L , $dL/dk = \infty$ at $k = 0$. This is analogous to the fixed-wing, Theodorsen theory which also has an infinite derivative of $k = 0$.

$$F = 1 - \frac{k\pi}{2}, \quad G = k \log \frac{k}{2} \quad (24)$$

This implies that no truly first-order model exists for small k . However, it is also known from Ref. 6 that the unsteady terms in dynamic inflow do not become crucial until $k \geq 5$. This is a large reduced frequency but is realistic even for low-frequency motions ($\omega = .5$) because v is typically of the order 0.1 ($\omega/v = 5$). Therefore, at these larger values of k , a first-order model may be adequate. As a further verification of the unsteady results, it would be interesting to exercise a transient wake analysis for the response of induced flow to a step input in blade pitch.

7. Summary

An actuator-disc theory has been used to obtain gains and time constants (i.e. the L and M matrices) for both 3-degree-of-freedom and 5-degree-of-freedom dynamic-inflow models. The following conclusions can be made:

1. In axial flow (e.g. hover), the gains are identical to those obtained from simple momentum theory, and they are independent of the radial lift distribution.
2. The apparent mass terms (the M matrix) for the simplest pressure distributions are identical to the apparent mass terms of an impermeable disc, but these values vary significantly with lift distribution.
3. Closed-form results are obtained for all elements of L at $\alpha = 90^\circ$ (axial flow), for all elements of L at $\alpha = 0^\circ$ (edgewise flow), and for the first column of L at all angles of incidence, α .
4. Numerical results for the elements of L at angles of incidence from 0° to 90° show that they are not strongly dependent upon lift distribution for $10^\circ < \alpha < 90^\circ$, although significant dependence does occur for $\alpha < 10^\circ$.
5. A 3-degree-of-freedom dynamic-inflow model is probably adequate for rotary-wing dynamics, and this model is expressed in analytic form in Table 4.
6. More work is required to substantiate the present dynamic-inflow model and to insure that wake contraction, finite number of blades, and

reduced-frequency effects will not substantially alter the dynamic-inflow characteristics.

REFERENCES

1. Amer, K.B., "Theory of Helicopter Damping in Pitch or Roll and a Comparison with Flight Measurements," NACA TN-2136, October 1948.
2. Sissingh, G.J., "The Effect of Induced Velocity Variation on Helicopter Rotor Damping in Pitch or Roll," Aeronautical Research Council Paper No. 101, Technical Note No. Aero. 2132, November 1952.
3. Carpenter, P.J. and Fridovitch, B., "Effect of Rapid Blade Pitch Increase on the Thrust and Induced Velocity Response of a Full Scale Helicopter Rotor," NACA TN-3044, November 1953.
4. Shupe, N.K., A Study of the Dynamic Motions of Hingeless Rotored Helicopters, Ph.D. Thesis, Princeton University, 1970.
5. Ormiston, R.A. and Peters, D.A., "Hingeless Helicopter Rotor Response with Nonuniform Inflow and Elastic Blade Bending," Journal of Aircraft, Vol. 9, No. 10, October 1972, pp. 730-736.
6. Peters, D.A., "Hingeless Rotor Frequency Response with Unsteady Inflow," Rotorcraft Dynamics, NASA SP-352, February 1974, pp. 1-12.
7. Crews, S.T., Hohenemser, K.H., and Ormiston, R.A., "An Unsteady Wake Model for a Hingeless Rotor," Journal of Aircraft, Vol. 11, No. 1, January 1974.
8. Ormiston, R.A., "An Actuator Disc Theory for Rotor Wake Induced Velocities," AGARD Specialists' Meeting on the Aerodynamics of Rotary Wings, Marseilles, France, September 13-15, 1972.
9. Joglekar, M. and Loewy, R., "An Actuator-Disc Analysis of Helicopter Wake Geometry and the Corresponding Blade Response," USAAVLABS Technical Report 69-66, December 1970.
10. Jones, J.P., "An Actuator Disc Theory for the Shed Wake at Low Tip Speed Ratios," MIT Aeroelastic and Structures Laboratory, Technical Report 133-1, 1965.
11. Loewy, Robert G., "A Two-Dimensional Approximation to the Unsteady Aerodynamics of Rotary Wings," Journal of the Aeronautical Sciences, Vol. 24, No. 2, February 1957.
12. Mangler, K.W., "Fourier Coefficients for Downwash of a Helicopter Rotor," Royal Aircraft Establishment Report No. Aero. 1958, May 1948.
13. Coleman, R.P., Feingold, A.M., and Stempin, C.W., "Evaluation of the Induced-Velocity Field of an Idealized Helicopter Rotor," NACA WR L-126, June 1945.

PRESSURE TERMS

m, n	$P_n^m(v)$	$\varphi_n^m(in)$	C_n^m	D_n^m	Purpose
0,1	v	$n \tan^{-1} \frac{1}{n} - 1$	$\frac{3}{4} C_T$	-	Gives desired thrust
0,3	$\frac{v}{2} (5v^2 - 3)$	$-\frac{n}{2} (5n^2 + 3) \tan^{-1} \frac{1}{n} + \frac{5}{2} n^2 + \frac{2}{3}$	$\frac{9}{8} C_T$	-	Hub correction for thrust
1,2	$-3v\sqrt{1-v^2}$	$\frac{3in\sqrt{1+n^2}}{\sqrt{1+n^2}} \tan^{-1} \frac{1}{n} - 3i\sqrt{1+n^2} + \frac{i}{\sqrt{1+n^2}}$	$-\frac{5}{8} i C_M$	$-\frac{5}{8} i C_L$	Gives desired moments
1,4	$-\frac{3}{2} v(7v^2 - 3)\sqrt{1-v^2}$	$-\frac{5}{2} in(7n^2 + 3)\sqrt{1+n^2} \tan^{-1} \frac{1}{n} + \frac{5}{6} i(21n^2 + 2)\sqrt{1+n^2} + \frac{i}{\sqrt{1+n^2}}$	$-\frac{9}{64} i C_M$	$-\frac{9}{64} i C_L$	Hub correction moments
2,3	$15v(1-v^2)$	$-15n(1+n^2) \tan^{-1} \frac{1}{n} + 15n^2 + 10 - \frac{2}{\sqrt{1+n^2}}$	$\frac{7}{128} C_{M2}$	$\frac{7}{128} C_{L2}$	Gives higher - harmonic loading

Table 1

L-Matrix for Edgewise Flow

Element	Uncorrected	Corrected	Vortex	Momentum
L_{11}	$\frac{1}{2} = .500$	$\frac{1}{2} = .500$	$\frac{1}{2} = .5$	$\frac{1}{2} = .5$
L_{22}	$-4*$	$-\frac{79}{16} = -4.938$	$-\frac{8}{3} = 2.7$	-2
L_{33}	0	0	0	-2
L_{31}	$\frac{3\pi}{8} = 1.178$	$\frac{15\pi}{64} = .736$	$\frac{1}{2} = .5$	0
L_{13}	$\frac{15\pi}{64} = .736$	$\frac{1395\pi}{3072} = 1.427$	1.0	0
L_{51}	$\frac{3}{5} = .600$	$-\frac{3}{7} = -.429$		
L_{42}	$-\frac{45\pi}{32} = -4.418$	$-\frac{2205\pi}{2048} = -3.382$		
L_{55}	$-6*$	+ multiply entries by $1/v$		
L_{24}	$\frac{105\pi}{128} = 2.577$	*limited numerical integration required		
* L_{15}, L_{35}, L_{44}	0			

Table 2

Elements of M-Matrix

Element	Uncorrected	Corrected
M_{11}	$\frac{8}{3\pi} = .8488$	$\frac{128}{75\pi} = .5432$
$M_{22} = M_{33}$	$-\frac{16}{45\pi} = -.1132$	$-\frac{256}{945\pi} = -.0862$
$M_{44} = M_{55}$	$-\frac{256}{1575\pi} = -.0517$	-
$M_{ij}, i \neq j$	0	0

Table 3

Analytic Forms of L-Matrix and M-Matrix

$[L] = \frac{1}{V}$	<table border="1" style="width: 100%; border-collapse: collapse;"> <tr> <td style="padding: 5px;">$\frac{1}{2}$</td> <td style="padding: 5px;">0</td> <td style="padding: 5px;">$\frac{15\pi}{64} \sqrt{\frac{1-\sin\alpha}{1+\sin\alpha}}$</td> </tr> <tr> <td style="padding: 5px;">0</td> <td style="padding: 5px;">$\frac{-4}{1+\sin\alpha}$</td> <td style="padding: 5px;">0</td> </tr> <tr> <td style="padding: 5px;">$\frac{15\pi}{64} \sqrt{\frac{1-\sin\alpha}{1+\sin\alpha}}$</td> <td style="padding: 5px;">0</td> <td style="padding: 5px;">$\frac{-4\sin\alpha}{1+\sin\alpha}$</td> </tr> </table>	$\frac{1}{2}$	0	$\frac{15\pi}{64} \sqrt{\frac{1-\sin\alpha}{1+\sin\alpha}}$	0	$\frac{-4}{1+\sin\alpha}$	0	$\frac{15\pi}{64} \sqrt{\frac{1-\sin\alpha}{1+\sin\alpha}}$	0	$\frac{-4\sin\alpha}{1+\sin\alpha}$
$\frac{1}{2}$	0	$\frac{15\pi}{64} \sqrt{\frac{1-\sin\alpha}{1+\sin\alpha}}$								
0	$\frac{-4}{1+\sin\alpha}$	0								
$\frac{15\pi}{64} \sqrt{\frac{1-\sin\alpha}{1+\sin\alpha}}$	0	$\frac{-4\sin\alpha}{1+\sin\alpha}$								
$[M] =$	<table border="1" style="width: 100%; border-collapse: collapse;"> <tr> <td style="padding: 5px;">$\frac{128}{75\pi}$</td> <td style="padding: 5px;">0</td> <td style="padding: 5px;">0</td> </tr> <tr> <td style="padding: 5px;">0</td> <td style="padding: 5px;">$\frac{-16}{45\pi}$</td> <td style="padding: 5px;">0</td> </tr> <tr> <td style="padding: 5px;">0</td> <td style="padding: 5px;">0</td> <td style="padding: 5px;">$\frac{-16}{45\pi}$</td> </tr> </table>	$\frac{128}{75\pi}$	0	0	0	$\frac{-16}{45\pi}$	0	0	0	$\frac{-16}{45\pi}$
$\frac{128}{75\pi}$	0	0								
0	$\frac{-16}{45\pi}$	0								
0	0	$\frac{-16}{45\pi}$								

Table 4

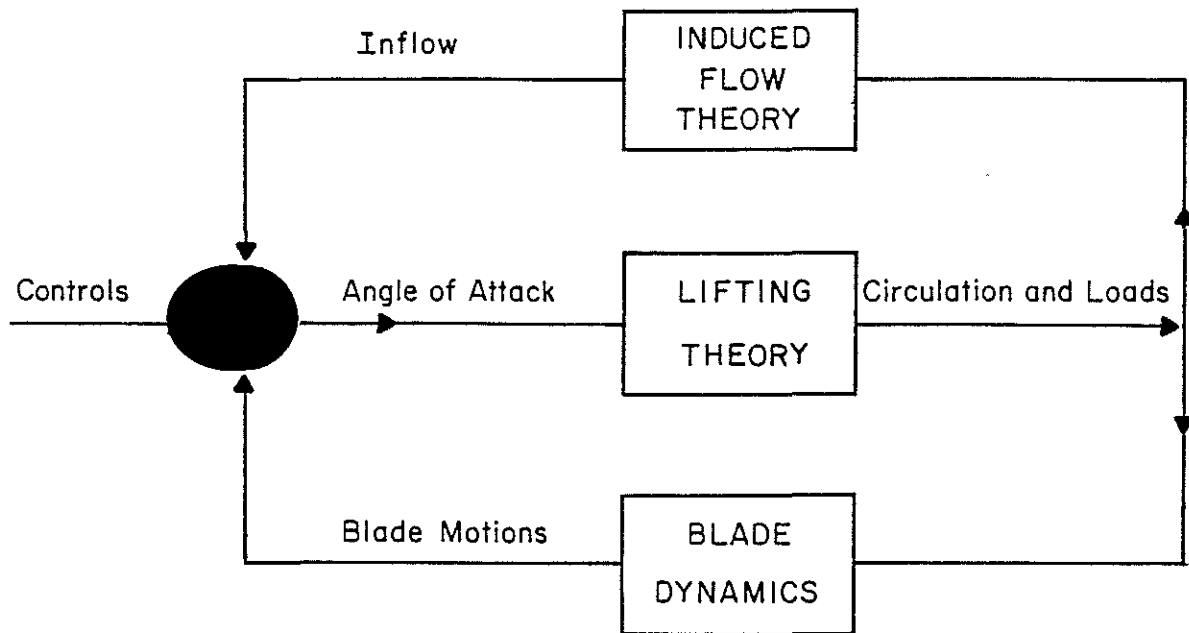


Figure 1. Block Diagram of Coupled Rotor and Induced-Flow Dynamics.

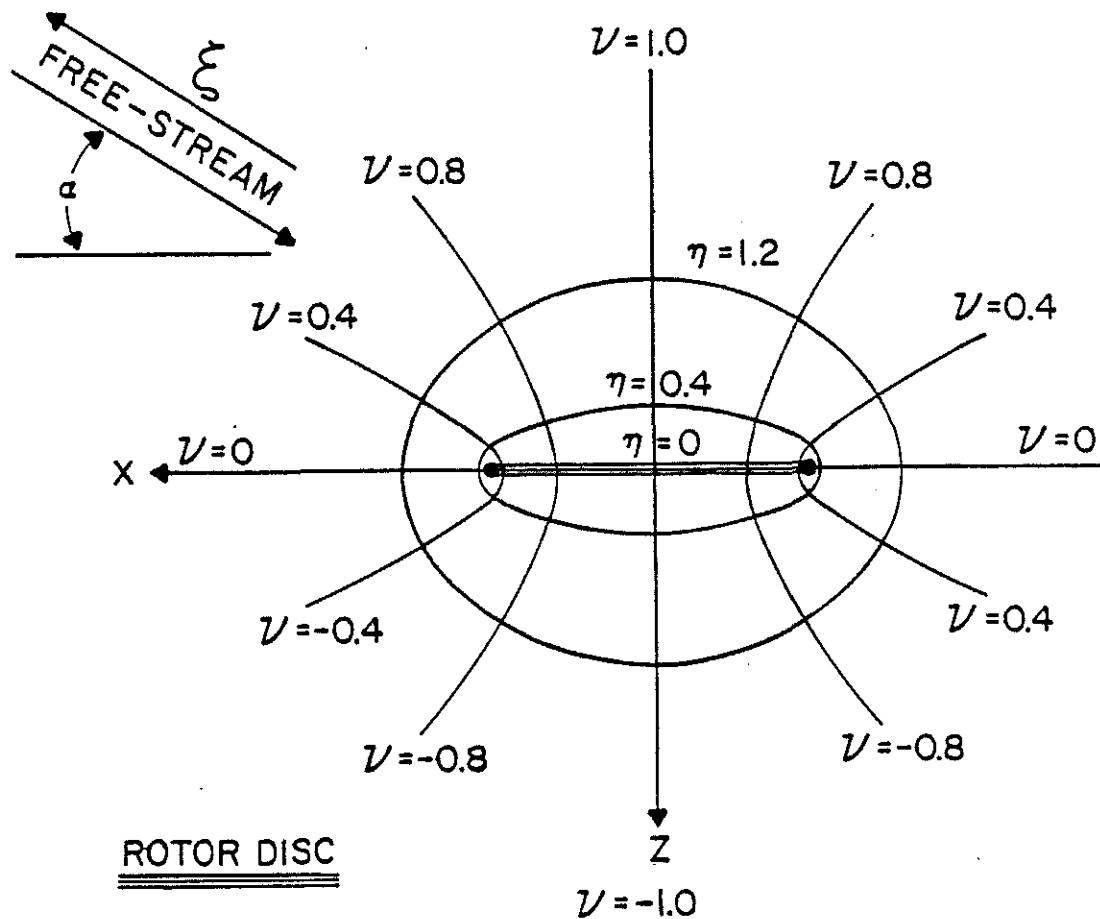


Figure 2. Ellipsoidal Coordinate System.

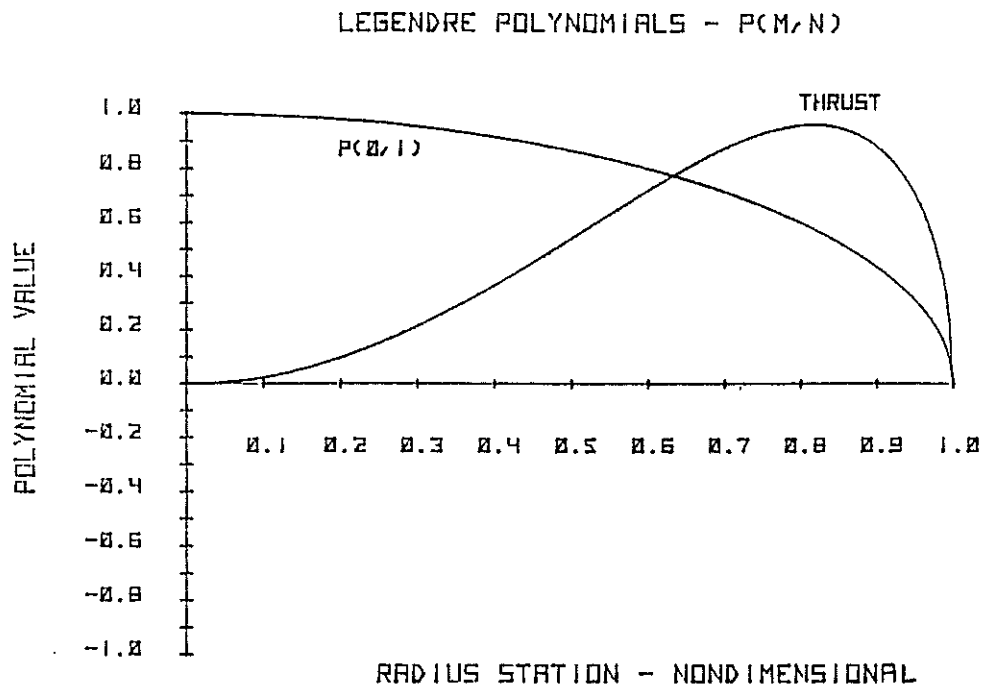


Figure 3. Corrected (Thrust) and Uncorrected (P_1^0) Lift Distributions for C_T .

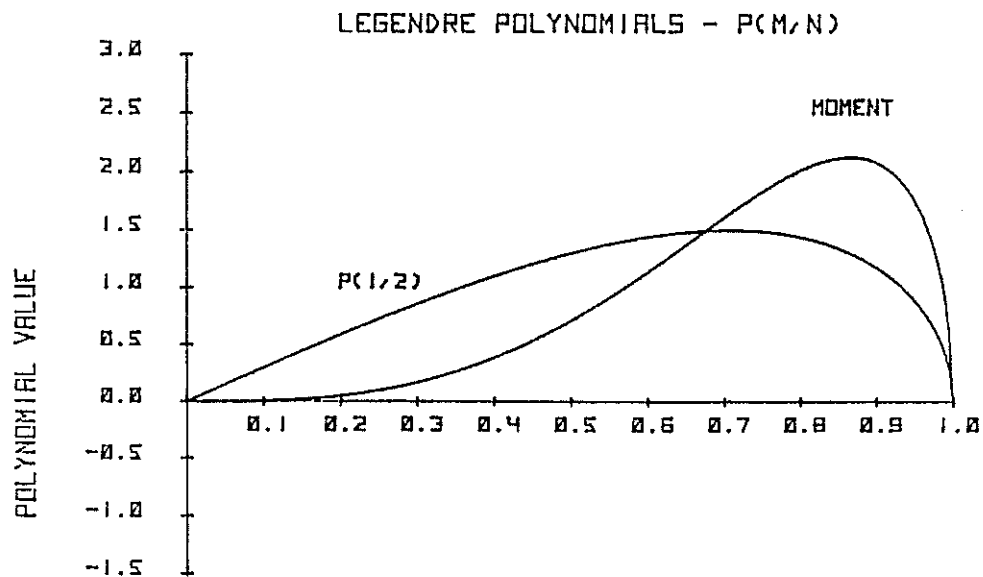


Figure 4. Corrected (Moment) and Uncorrected (P_2^1) Lift Distributions for C_L or C_M .

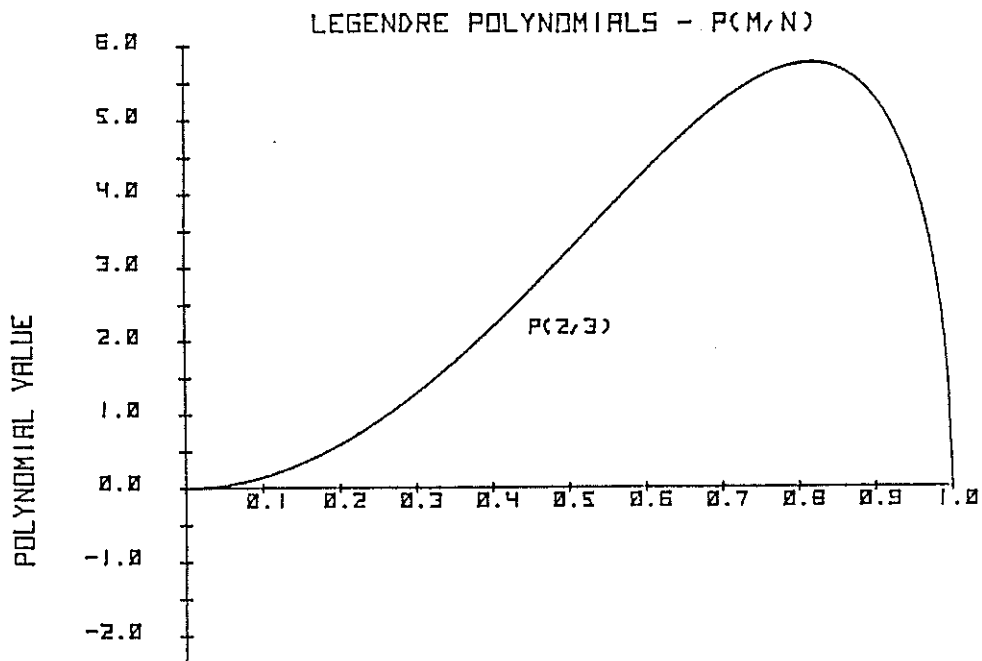


Figure 5. Lift Distribution (P_3^2) for C_{L2} or C_{M2} .

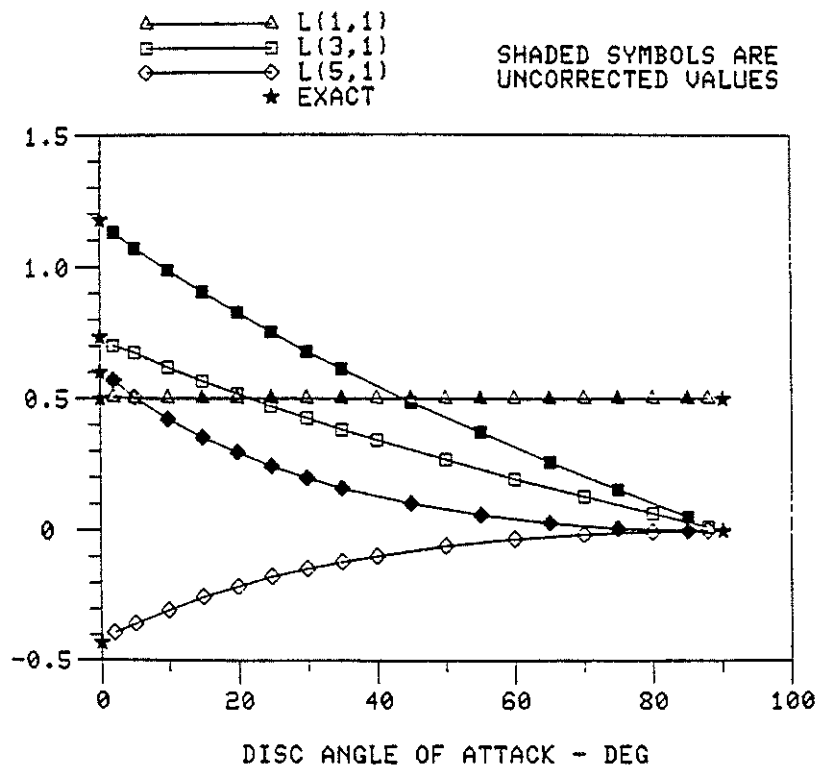


Figure 6. First Column of L-Matrix (C_T).

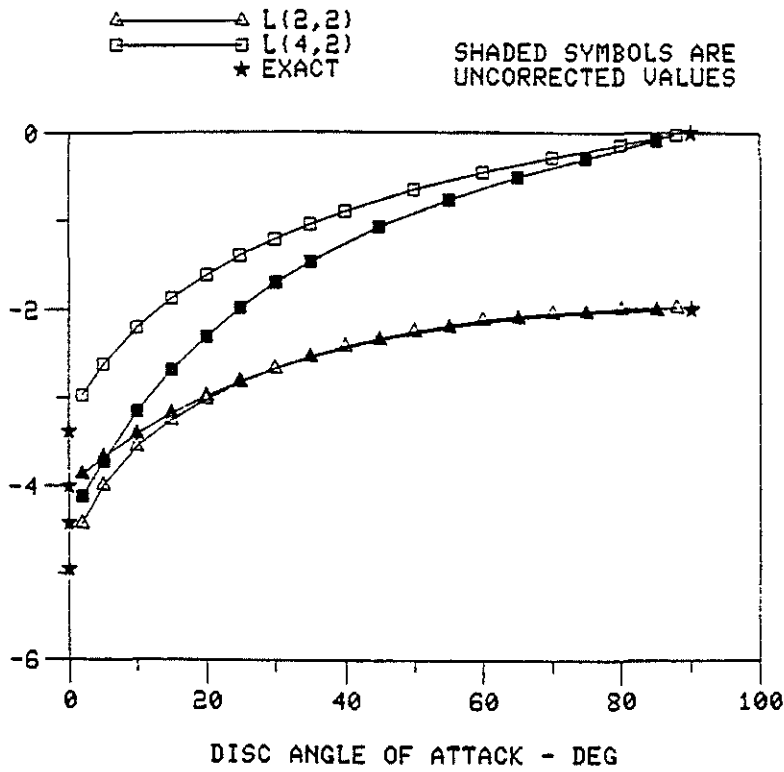


Figure 7. Second Column of L-Matrix (C_L).

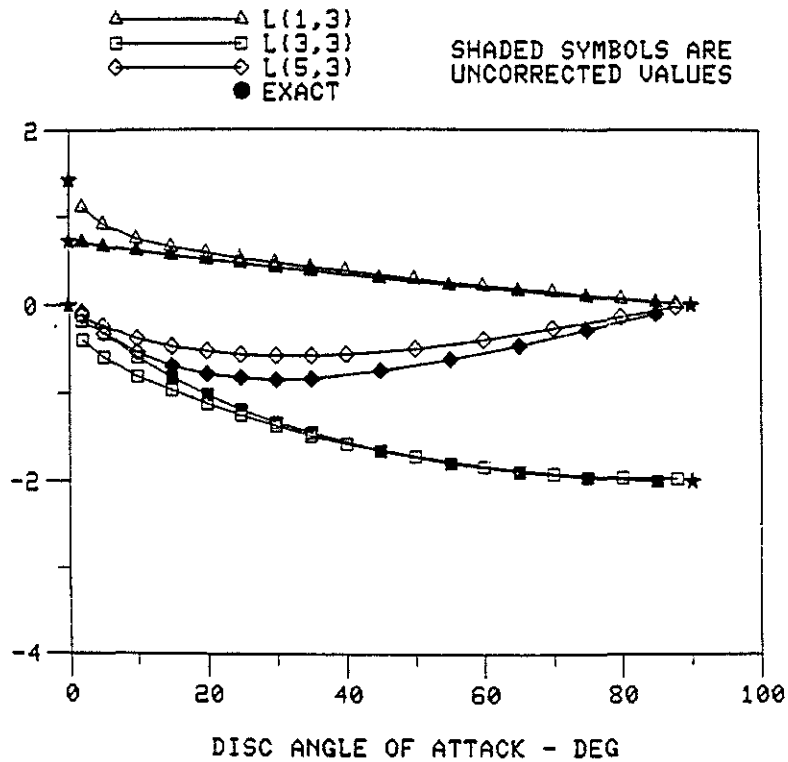


Figure 8. Third Column of L-Matrix (C_M).

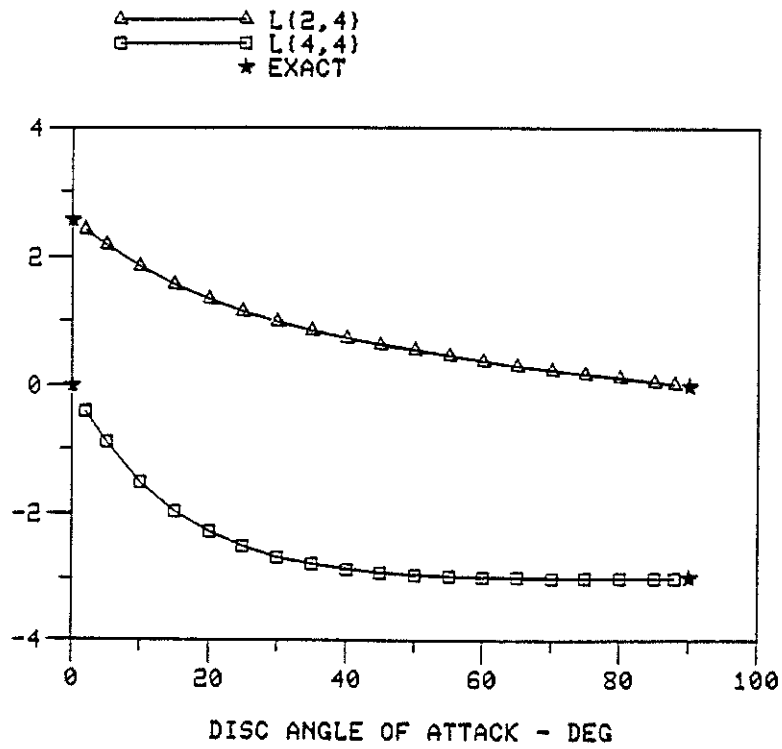


Figure 9. Fourth Column of L-Matrix (C_{L2}).

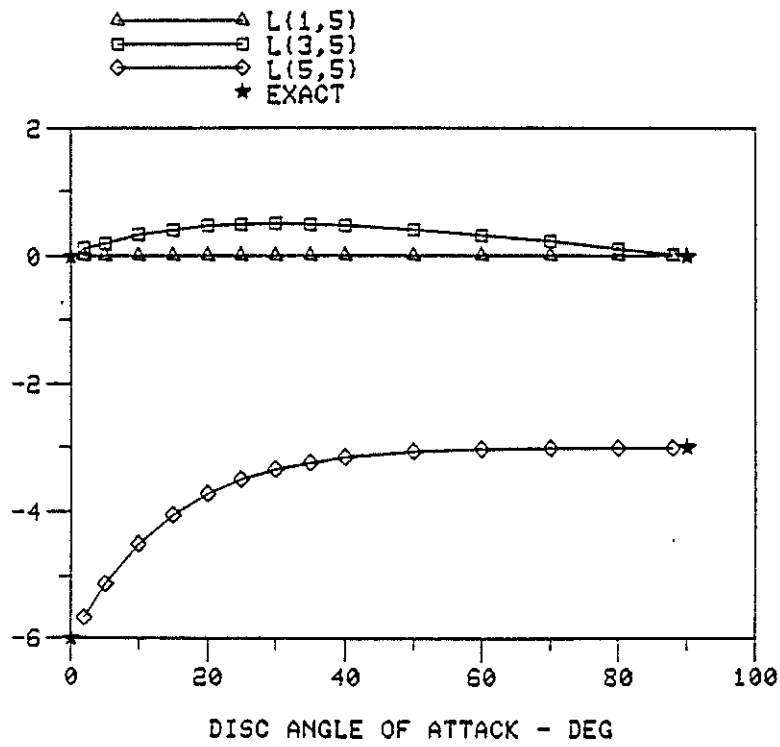


Figure 10. Fifth Column of L-Matrix (C_{M2}).